Structure functions in nocturnal atmospheric boundary layer turbulence

Eliezer Kit [1,2,*], Eli Barami [3,4] and H. J. S. Fernando [2,5]

[1]*School of Mechanical Engineering, Tel Aviv University, Tel Aviv 69978, Israel*
[2]*Department of Civil and Environmental Engineering and Earth Sciences, University of Notre Dame, Notre Dame, Indiana 46530, USA*
[3]*Department of Mechanical Engineering, Ben-Gurion University of the Negev, Beer-Sheva 84105, Israel*
[4]*Soreq Nuclear Research Center, Yavne 8180000, Israel*
[5]*Department of Aerospace and Mechanical Engineering, University of Notre Dame, Notre Dame, Indiana 46530, USA*

This paper analyzes odd and even higher-order moments for longitudinal velocity increment $\Delta u(x, r)$, where x is the longitudinal coordinate and r is the separation distance, based on the canonical and a modified normalization for skewness of longitudinal velocity derivative $\partial u/\partial x$. Two types of data were used, stably stratified turbulence data from the nocturnal atmospheric boundary layer taken during the Mountain Terrain Atmospheric Modeling and Observations field campaign and from the direct numerical simulation of homogeneous and isotropic turbulence in a box at four Reynolds numbers and four different grid resolutions. Third moment data normalized by the same moment of third order for modulus $|\Delta u(x, r)|$ representing modified skewness of the velocity increment showed a better collapse at all Reynolds numbers in the *inertial* and *viscous* subranges than canonical normalized skewness with normalization parameter $\langle(\Delta u(x, r))^2\rangle^{3/2}$, where $\langle\cdot\cdot\rangle$ represents the ensemble average. The analysis also considered odd pth-order classical structure functions $\langle\Delta u(x, r)^p\rangle$ with Kolmogorov-theory based normalization $\langle\Delta u(x, r)^p\rangle/(\varepsilon r)^{p/3}$ for the inertial subrange, where ε is the rate of dissipation, and a modulus-based structure function $\langle|\Delta u(x, r)|^p\rangle/(\varepsilon r)^{p/3}$. Both types of structure functions of order $p = 1$–6 were computed using different normalizations, and corresponding scaling exponents were assessed for the inertial and viscous subranges. Scaling for modulus-based structure functions in the viscous subrange was identified as $\langle|\Delta u(x, r)|^p\rangle \propto r^{p\cdot(5/6)}$. In the viscous subrange, the velocity increment varied linearly with r for the classical third moment $\langle\Delta u(x, r)^3\rangle \propto r^3$ based on the velocity increment while the classical fifth moment $\langle\Delta u(x, r)^5\rangle$ did not provide any meaningful scaling exponent. A plausible qualitative explanation linking these effects to anisotropy of nocturnal stratified turbulence is proposed.

I. INTRODUCTION

In his seminal work, Kolmogorov [1] proposed two hypotheses or postulates on turbulence.

(1) The Kolmogorov self-similarity hypothesis (KSSH) enabled one to express, based on dimensionless considerations, the structure function $L_p(r)$ defined as a moment of any order p of the velocity increment Δu at a separation r as a function of ε [mean turbulent kinetic energy (TKE) dissipation rate] and r as $L_p(r) = (\Delta u)^p \propto (r\varepsilon)^{p/3}$. This is strictly appropriate for homogeneous isotropic turbulence (HIT), a theoretical abstraction that can be made pragmatic by introducing the postulate of local isotropy (PLI) as below.

---

*Corresponding author: elikit@gmail.com

(2) The PLI assumes that, far from boundaries and external forces applied at large scales, turbulence loses memory as it cascades down from large to smaller scales, wherein turbulence becomes locally isotropic and therefore the KSSH is applicable. This cascading region (inertial subrange) is suitably separated from the regions of larger TKE containing scales and much smaller viscous dissipation scales. The dissipation subrange is also locally isotropic, but viscous influence therein engenders scaling laws different from those of the inertial subrange.

In most subsequent studies the KSSH was tested for the inertial subrange, and an anomalous exponent instead of the Kolmogorov $p/3$ scaling was observed. To explain and predict such anomalies, a large number of models have been suggested, for example, extended self-similarity hypothesis, refined KSSH (RKSH), and fractal models. Most of them included the intermittency, especially that of ε. There is strong evidence from field, laboratory, and direct numerical simulation (DNS) studies to suggest that ε is associated with small-scale turbulence structures distributed unevenly in space, being confined to a smaller fraction of space determined by the size of small eddies [2,3], thus undermining the KSSH [1]. As such, it is well known that the scaling exponents differ dramatically from the Kolmogorov $p/3$ exponents, and this disparity increases with both p and r^{-1} [4], revealing non-Gaussian behavior [5] in HIT. As well, real turbulent flows include anisotropic forcing and boundary conditions, particularly in stratified fluids [6–8], and this anisotropy may penetrate to *inertial* and, perhaps, *dissipation* or *viscous* subranges. This perfusion of anisotropy obviously puts the PLI into question, as discussed below.

Literature of DNS studies on HIT at high Taylor microscale Reynolds numbers Re_λ, e.g., [9–11], are voluminous. Benzi *et al.* [12,13] experimentally investigated scaling laws using grid flows and at the center of jet and wake flows. Extended self-similarity (ESS) based on the use of the third-order structure function for normalization instead of separation r was applied to determine anomalous scaling exponents; significant anomalies were observed, in good agreement with peer studies. Instead of third-order longitudinal structure function $L_3(r) = \langle (\Delta u(x, r))^3 \rangle$, an alternative function $L_3^*(r) = \langle |\Delta u(x, r)|^3 \rangle$ was proposed [12–14]. As expected in the viscous subrange for very small normalized separations $r/\eta \approx 1$, where η is the Kolmogorov scale, the velocity difference $\Delta u(x, r)$ is regular, causing both the velocity difference and its modulus to be approximately proportional to r. Similar results were obtained by the same group [15,16] and others [17–23]. Most efforts by Benzi *et al.* [15,16] and She and Leveque [19] were focused on identifying the most appropriate model for anomalous scaling exponents.

Sreenivasan and Dhruva's [24] measurements in the surface layer of the atmospheric boundary layer (ABL) reached very high Taylor microscale Reynolds numbers Re_λ (10 000 to 20 000), but the PLI could not be validated, which was ascribed to the presence of mean shear. Laboratory experiments with homogeneous shear flow by Warhaft and coworkers [25–27] showed unambiguously that return to isotropy expected at small scales does not occur either at lower $\mathrm{Re}_\lambda \sim \mathrm{O}(100)$ [25] or at higher $\mathrm{Re}_\lambda \sim \mathrm{O}(1000)$ numbers [26], which again was ascribed to shear. To quote [26] "The results show that PLI is untenable, both at the dissipation and inertial scales, at least to $R_\lambda \sim 1000$, and suggest it is unlikely to be so even at higher Reynolds numbers." In grid flows without shear [30], however, the isotropy at small scales could be realized, and thus the expected praxis of zero odd transversal structure functions was manifested.

Effects of shear on similarity laws, scaling laws, intermittency, and anisotropy of small scales have been further studied in laboratory experiments and DNS of channel flow turbulence, wall bounded turbulence, homogeneous shear flows, and nonhomogeneous turbulence [28–34]. With regards to similarity laws, in HIT the celebrated KSSH was replaced by the RKSH [5] to account for intermittency of ε, which was found appropriate and sound away from the wall (logarithmic) region of the boundary layer. Near the wall, where shear is strong, the classical RKSH was not valid, and an "alternative RKSH" [29] has been proposed to account for stronger intermittency. Therein, the PLI at small scales was violated as anisotropy penetrated the smallest scales, scaling anomalies became pronounced, and scaling exponents deviated from the Kolmogorov counterpart $p/3$ more remarkably than in HIT. At intermediate distances from the wall, double scaling could be obtained where both RKSH and alternative RKSH anomalous exponents appear to coexist.

In [35–40], $SO(3)$ formalism was used for systematic decomposition of structure and/or correlation functions in spherical harmonics to separate isotropic and anisotropic contributions. This decomposition enables the determination of scaling exponents in the isotropic and anisotropic sectors in the presence of strong and weak shear, thus following possible decay of anisotropic contributions at small scales. Interestingly, measurements in homogeneous shear flow by Casciola, Gualtieri, Jacob, and Piva [36,37] found that anisotropic contributions in weak shear waning at a relatively fast rate while under strong shear the anisotropy keep a significant presence up to viscous scales, thus violating the PLI [37]. The latter fine-scale anisotropy is accompanied by stronger intermittency and stronger deviation of scaling exponents from HIT. These authors [37] conclude: "It has always been believed that turbulence in fluids can achieve a universal state at small scales with fluctuations that, becoming statistically isotropic, are characterized by universal scaling laws. In fact, in different branches of physics it is common to find conditions such that statistical isotropy is never recovered and the anisotropy induced by large scale shear contaminates the entire range of scales up to velocity gradients."

Arad *et al.* [41] conducted ABL surface layer measurements at very high Re_λ (10 000–20 000), and $SO(3)$ rotation groups were employed to determine scaling exponents in different isotropic and anisotropic sectors. The contributions of anisotropic sectors were small, indicating weak effects of shear. Nevertheless, the accounting for these anisotropic contributions significantly improved the correspondence between experimental data and the analytic fit. A general theory explaining the decomposition of structure and correlation functions (by projections on the spherical harmonics) as well as determination of scaling exponents in isotropic and anisotropic sectors are presented in [42–45].

Notwithstanding the above advancements with regard to shear flows, studies on possible penetration of anisotropy into small scales of stable stratified flows are far fewer. A few high-quality experimental studies [46–49] augmented by DNS [50] unambiguously show that, much the same way as for shear, strong stable stratification begets large anisotropies in the mean-square strain rates $\partial v/\partial x$ and $\partial w/\partial x$ relative to $\partial u/\partial x$. Studies of stably stratified grid-generated HIT [46,47] report "an unexpected rapid onset of anisotropy in the small scales," which is true for *uniformly sheared thermally stratified* turbulent flow [48,49]. A combination of shear and stratification, especially for decaying turbulence, is expected to increase the propensity for small-scale anisotropy compared due to either shear or stratification alone.

The outcomes of past research discussed above will be used in Sec. III to argue that the anomalous scaling for structure functions obtained during fine-scale hot-film measurements of turbulence in the nocturnal ABL during the field campaigns of the Mountain Terrain Atmospheric Modeling and Observations (MATERHORN) program [51,52] is possibly due to stratification effects and not due to shear (since the measurements were conducted *well away* from the wall layer). An intriguing observation of MATERHORN was the intermittent appearance of strong bursts at nighttime (stably stratified conditions) at smaller scales characterized by ephemeral rise of velocity fluctuations and simultaneous increase of ε by orders of magnitude. The separation of data into "burst" and "no-burst" time intervals based on a chosen threshold of ε enabled processing of both burst and no-burst datasets independently. The dataset without bursts can follow classical Kolmogorov turbulence if the effects of stratification can be considered insignificant. The datasets with bursts behaved differently in that the TKE spectral shape exhibited bumps in the inertial subrange [53].

This paper concerns a modified normalization for *higher odd moment*s of longitudinal velocity increment $\Delta u(x, r)$ built upon the normalization proposed in [52] for *skewness* of the longitudinal velocity derivative $\partial u/\partial x$. No-burst datasets from MATERHORN were used along with those from limited DNS computations of HIT.

II. METHODOLOGY

An intriguing effect observed in the nocturnal ABL is the appearance of episodic but puissant turbulence or bursts. Arguably, this may occur either in HIT or anisotropic turbulent flows subject to

external forcing such as stratification, rotation, or electromagnetic forces that promote anisotropy. These factors may magnify the deviation of the probability density functions (PDFs) from Gaussian, but not necessarily increase its asymmetry present in HIT due to nonlinearity. It is well known that the PDF of velocity derivatives in HIT is skewed, leading to a considerable negative third moment (vis-à-vis zero for the Gaussian distribution) of the longitudinal velocity derivative; this explains the appearance of the generation term in the vorticity equation that causes production of enstrophy [54].

Enstrophy production and intermittency in turbulent flows occur due to two independent effects: in the HIT case, turbulence is skewed at the intermediate (inertial subrange) and small (dissipation range) scales, thus magnifying the enstrophy flux to small scales. In addition to the presence of stretched vortex sheets and vortex tubes that is associated with strong intermittency at very small scales of HIT, breaking of small-scale random internal gravity waves in (anisotropic) stably stratified turbulence may also lead to enstrophy generation and intermittency. The range of scales at which such breaking occurs and associated dynamics are yet to be understood (and the separation of internal waves from turbulence continues to be a vexing problem).

The nocturnal ABL is a case where stability evolves overnight due to radiative cooling at a pace slower than the time scale of turbulence, leading to a myriad of turbulence-related phenomena that were studied during MATERHORN (2011–2016) field experiments. A probing system was deployed for this purpose, the details of which are given in [52,55]. The finer scales therein were captured with a sonic- and hot-film anemometer dyad (dubbed the "combo" probe) placed on a horizontal pole at 6-m height of a 32-m-high tower (labeled ES-2) equipped with an array of sonics and thermocouples at various levels. This system is described in [52] and the MATERHORN experiment is described in [51]. The data encompassed a variety of flow types that appear over different phases of the diurnal cycle, but careful winnowing could identify data that fit the rubric of stratified shear flows, which emerged from a katabatic flow draining from the nearby Granite Mountain.

After careful processing of sonic records of ES-2, the 90-min period of katabatic flow starting from 22:00 MDT[1] on October 19, 2012 was selected for stratified shear flow studies. Prior to the selected time interval, the wind speed rapidly increased from ≈ 1 to $\approx 4\,\mathrm{m/s}$ at the height of the combo probe. The wind direction changed from its usual oscillations before 22:00 MDT to a nearly constant direction, resembling a stratified parallel shear flow. Thereafter, the winds changed quite rapidly between 23:30 MDT and midnight [52]. Although mean quantities were quasisteady during the selected period 22:00–23:30 MDT, careful inspection of turbulence statistics showed considerable variability. An analysis for identification of approximately homogeneous subintervals enabled focusing on structure function analysis in the subinterval SI_{devd})22 : 50–23 : 10 MDT). This subinterval was considered as fully developed turbulence since flow variations were modest and appearance of bursting events was very limited (less than 2% of the time). More details can be found in [52,56].

To augment, three-dimensional homogeneous and stationary turbulence was studied using high-resolution DNS in a periodic box with up to 1024^3 grid points. A pseudospectral code with large-scale random forcing and triply periodic boundary conditions was used. The white-in-time Gaussian forcing was placed in the range of scales $1 \leqslant k \leqslant \sqrt{6}$. The DNS was carried out at four grid resolutions, yielding $Re_\lambda = 139, 201, 264$, and 383. Details of the numerical scheme are given in [11].

III. RESULTS

A. Datasets from field campaign and DNS

The datasets revealed strong bursts characterized by short-term increase of velocity fluctuations and simultaneous increase of ε by orders of magnitude. The separation between burst and no-burst

---

[1]Mountain daylight time (local time).

time intervals was based on a threshold for ε, as in [52]. The data without bursts followed the Kolmogorov $-5/3$ law whereas those with bursts showed bumps in the TKE spectra. Since no-burst periods resembled Kolmogorov turbulence, it was decided to test various features of intermittency using no-burst field data sets and DNS of HIT turbulence. The analysis focused, *inter alia*, on the modified normalization suggested in [53], the effects of varying Reynolds number, and the scaling exponents in various subranges, e.g., inertial and viscous. The modified normalization is based on [53], where the second-order denominator $\overline{((\partial u/\partial x)^2)}^{3/2}$ of the canonical skewness of the longitudinal velocity derivative $\partial u/\partial x$ is replaced by the same third-order moment of its modulus $\overline{|\partial u/\partial x|^3}$ to define an alternative descriptor for intermittency studies. In our work described below, modulus based normalizations are extended for odd structure functions of higher orders $p = 3, 5,$ and 7.

B. Normalized odd structure functions in DNS

The following discussion deals with longitudinal structure function $L_p(r)$ of order p; $L_p^*(r)$ is the same function based on the absolute values of the longitudinal velocity increment $\Delta u(x, r) = u(x + r) - u(x)$, where r is the separation distance:

$$L_p(r) = \langle (\Delta u(x, r))^p \rangle \quad L_p^*(r) = \langle |\Delta u(x, r)|^p \rangle. \tag{1}$$

The moments of the velocity increment in the canonical form are

$$H_p(r) = L_p(r)/[L_2(r)]^{p/2}, \quad H_p^*(r) = L_p^*(r)/[L_2(r)]^{p/2}. \tag{2}$$

We dealt mostly with odd moments, $p = 3, 5,$ and 7, and, following [53], considered *modified* moments $\tilde{H}_p(r) = L_p(r)/L_p^*(r) = H_p(r)/H_p^*(r)$ along with the moments obtained using *canonical* normalization presented in (2). Note that, at small separations r, the normalized structure-function based velocity *increments* become the moments of the velocity *derivative*. For example, at $p = 3$, velocity derivative skewness can be retrieved as $H_3 = S = \langle (\partial u/\partial x)^3 \rangle / \langle (\partial u/\partial x)^2 \rangle^{3/2}$, which was the focus in [53].

The normalized canonical moments for $p = 3, 5,$ and 7 at all four Re_λ numbers in DNS are given in Fig. 1, and the modified moments $\tilde{H}_p(r)$ for $p = 3, 5,$ and 7 are presented for comparison in Fig. 2 where the separation scale r is normalized by the Kolmogorov length scale η.

Note the two striking differences between Figs. 1 and 2. Plots for two highest Re_λ practically collapse in Fig. 2 in both viscous ($r/\eta < 10$) and inertial (50–200) subranges while they obviously differ systematically in Fig. 1 in all subranges. The upper boundary of the inertial subrange (Fig. 1) depends significantly on Re_λ and is about 300 for the highest $Re_\lambda = 383$, and it reduces remarkably at lower Re_λ due to the reduction of separation between large and dissipating scales. At larger scales, universal scaling is not expected given their dependence on boundary conditions and details of large-scale forcing. In the inertial subrange, all modified *moments* (Fig. 2) remain approximately constant, while canonical *moments* (Fig. 1) decline with an approximately constant slope. The slope increases with the order p of moments, as was observed by [12].

C. Comparisons of various structure function moments in experiments and simulations

The results of Sec. III B for odd moments led us to conduct a detailed comparison of normalized (canonical and modified) moments obtained via DNS and field experiments. We started with the third moment due to its relation to the corresponding structure function, for which classical theoretical results based on the Kolmogorov equation [5] are available. All meaningful field results were obtained for the no-burst events. Events with burst did not provide sensible plots for interpretation.

In Figs. 3 and 4, respectively, the results are presented for third- and thfifth-order canonical and modified structure functions; see Eqs. (1) and (2) for definitions. Obviously, the modified moments make sense only for odd moments. It is worth noting that canonical moments can be sensitive to
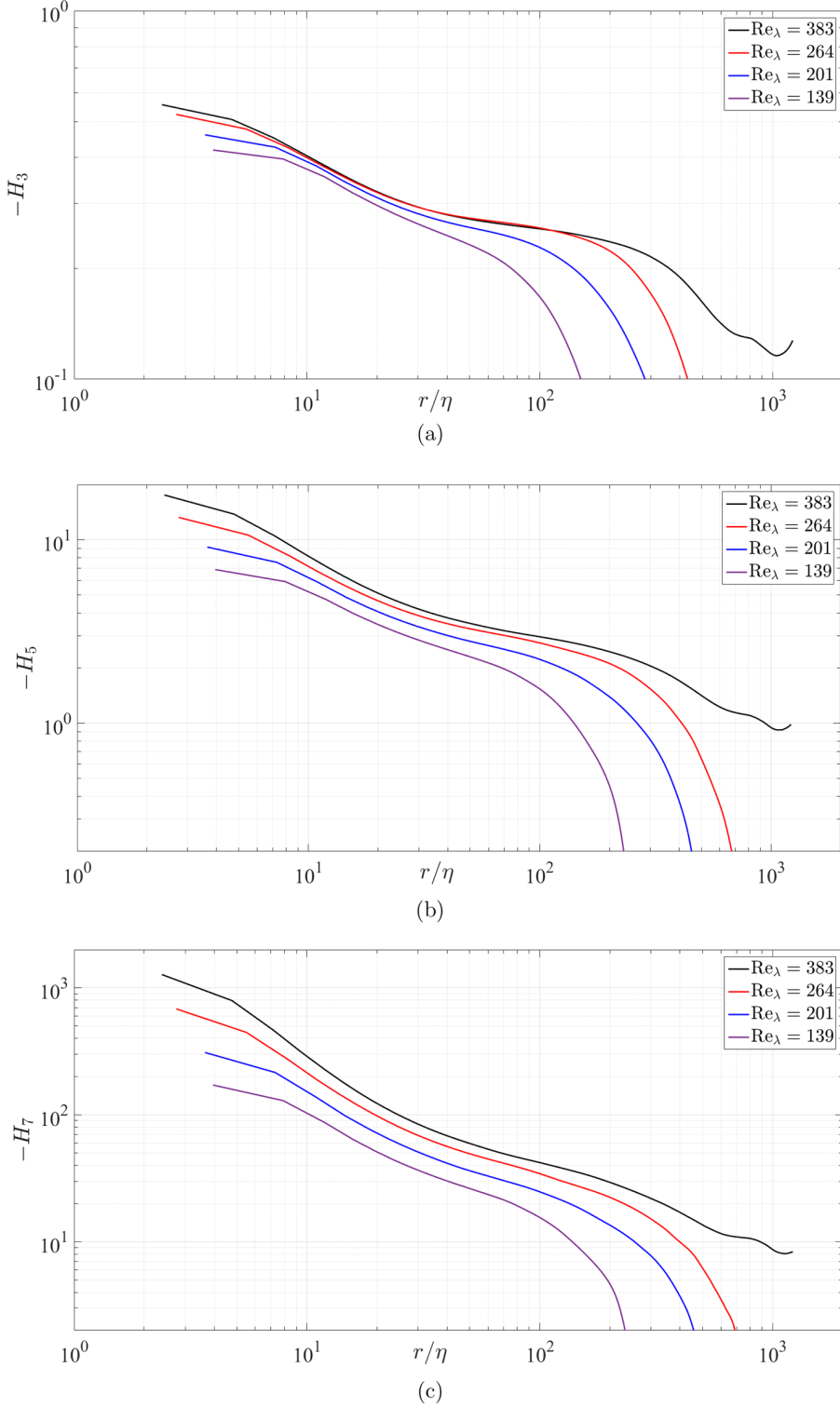
FIG. 1. Canonical odd moments for all four datasets obtained in DNS: (a) third, (b) fifth, and (c) seventh moments.
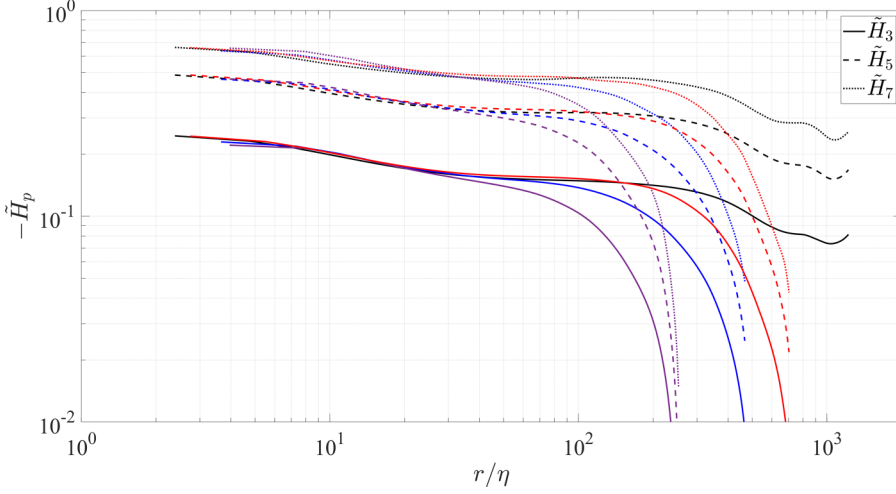
FIG. 2. Modified moments for all four DNS datasets. Color coding is the same as in Fig. 1.

intermittency, as it may affect differently the moments in the numerator and denominator, which are of different order. It is noted in [53] that odd moments of the same order $L_p(r)$ and $L_p^*(r)$ depend similarly on the intermittency and, therefore, normalization using $L_p^*(r)$ can significantly decrease the influence of intermittency on the scaling exponent.

Figure 3(a) indicates almost perfect agreement between the experimental and DNS canonical moments in the inertial range, which decay as $H_3 = L_3/(L_2)^{3/2} \sim (r/\eta)^{-0.1}$. Since this appealing result was obtained in two physically different systems, at notably different characteristic Re_λ, it was necessary to analyze these outcomes with care to elicit the similarity of turbulence structures.

In the viscous subrange, at small normalized separations $r/\eta < 10$, the results of Fig. 3(a) show different behavior, and the scaling exponents are even of different sign for field and DNS data.

The DNS-field $\tilde{H}_3$ comparisons shown in Fig. 3(b) indicate that in the inertial subrange the structure functions are *qualitatively* in very good agreement. The scaling exponents at the highest Re_λ, in spite of being very low (3.6%), are practically the same for DNS and field data. The *quantitative* agreement is less satisfactory compared to the canonical third moment. In contrast to scaling exponents in the inertial subrange, Fig. 3(a) shows that in the viscous subrange the scaling exponents for the third canonical moments are different for the field and DNS data. Similar trends are evident in Fig. 3(b), again indicating exponents of different signs for field and DNS data in the viscous subrange.

Increasing the rank of the moments inevitably decreases the accuracy since the effect of greater velocity increments becomes more substantial and the resolution worsens due to their lower probability. Therefore, employing odd moments higher than the fifth seemed unreasonable. The canonical and modified fifth moments calculated for field and DNS data are presented in Figs. 4(a) and 4(b), respectively. In the inertial range, they are in almost perfect agreement with regard to slope (–0.25) but not the amplitude. For example, in Fig. 4(a), at $r/\eta = 100$, the amplitude is 4.3 for field and 3 for DNS data. In the viscous subrange ($r/\eta < 10$), however, the slope is negative (–0.35) in DNS [Fig. 4(a)] and fluctuating in the field data; this contrasts field observations for the third canonical moment, wherein a slope of about 0.5 was noted [Fig. 3(a)].

In the inertial subrange, for fifth-order modified moments obtained using field and DNS data [Fig. 4(b)], the slope is slightly positive ($\approx 1.5\%$ for both). In the viscous subrange, the slope is moderately negative (–9.5%) for DNS, but is fluctuating for field data as in the case of fifth canonical moments in Fig. 4(a).
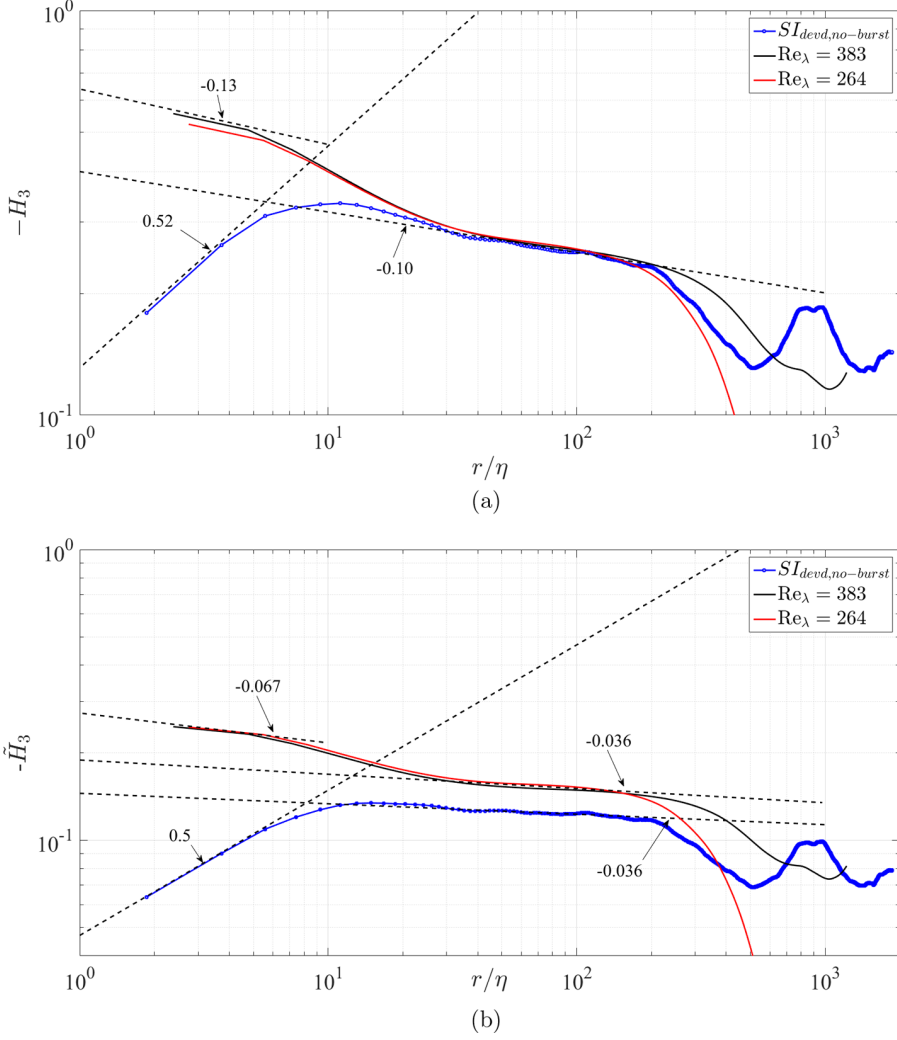
FIG. 3. Comparison of the third canonical (a) and modified (b) moments obtained in the field campaign [51,52] with $\mathrm{Re}_\lambda = 1200$ and DNS conducted for the two highest $\mathrm{Re}_\lambda = 264$ and 383. The periods indicated in the legends are for time periods without bursts, determined according to the methodology of [52].

Let us first consider modified structure functions of the odd third- and fifth-order moments since their expressions include the moments of the same order in numerator and denominator. It has been widely assumed [11–14,20–22] that third-order moments based on the velocity increment and its modulus have very similar scaling in the inertial and viscous subranges, and in each the exponents differ only by a few percent. Our (nearly HIT) DNS data confirm this assumption, but field data (stratified turbulence in the nocturnal boundary layer) show this trend only in the inertial subrange; in the viscous subrange, the scaling exponents differ substantially to the extent that even the sign of the slope can be different between DNS and field. Since the expectation for the viscous subrange was a linear dependence of velocity increment on separation r, this result was highly unexpected. The results for the fifth-order modified structure function in the viscous subrange was even more puzzling since the moments were randomly fluctuating without a firm dependence on separation r.
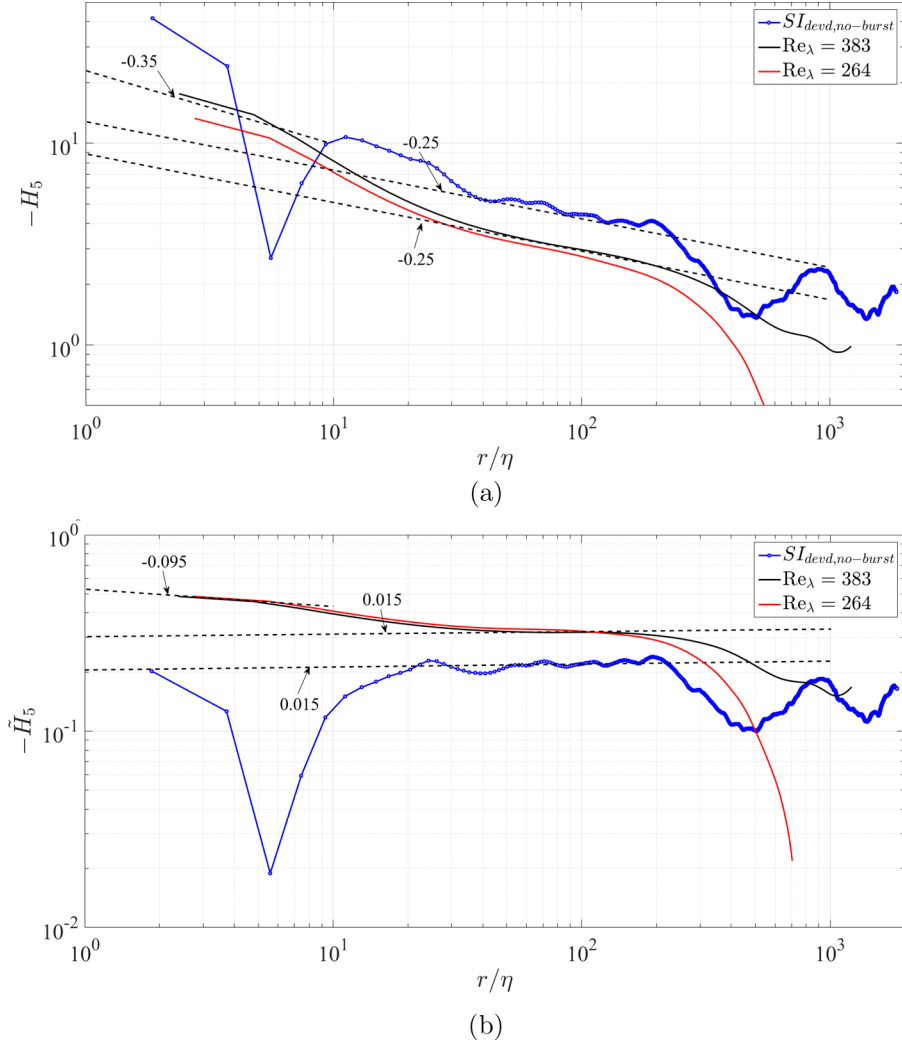
FIG. 4. Comparison of fifth canonical moments (a) and modified moments (b) obtained in the field and DNS.

Unexpectedly, in the viscous subrange, the canonical third- and fifth-order moments [Figs. 3(a) and 4(a)] normalized by the power $p/2$ of the second moment (that lineages to KSSH) behaved very similarly to the modified moments of the same order [Figs. 3(b) and 4(b)]. In particular, the scaling exponents of the third-order moment were practically the same (0.50 for modified and 0.52 for canonical moments) and the fifth-order canonical moment fluctuated randomly similarly to the case of the fifth-order modified moment. Recall that the modified normalization was suggested in [53] to ameliorate intermittency effects by using moments of the same order in the numerator and denominator. Therefore, the expectation was that due to different normalization the canonical and modified moments will behave differently in the viscous subrange. To clarify these findings, the structure functions $L_p(r)$ normalized using Kolmogorov inertial subrange scaling $(r\varepsilon)^{p/3}$ were investigated.

The second- and third-order structure functions, which are directly related to turbulence dynamics and appear in the Kolmogorov equation [1], are considered first. In Fig. 5, the KSSH-normalized
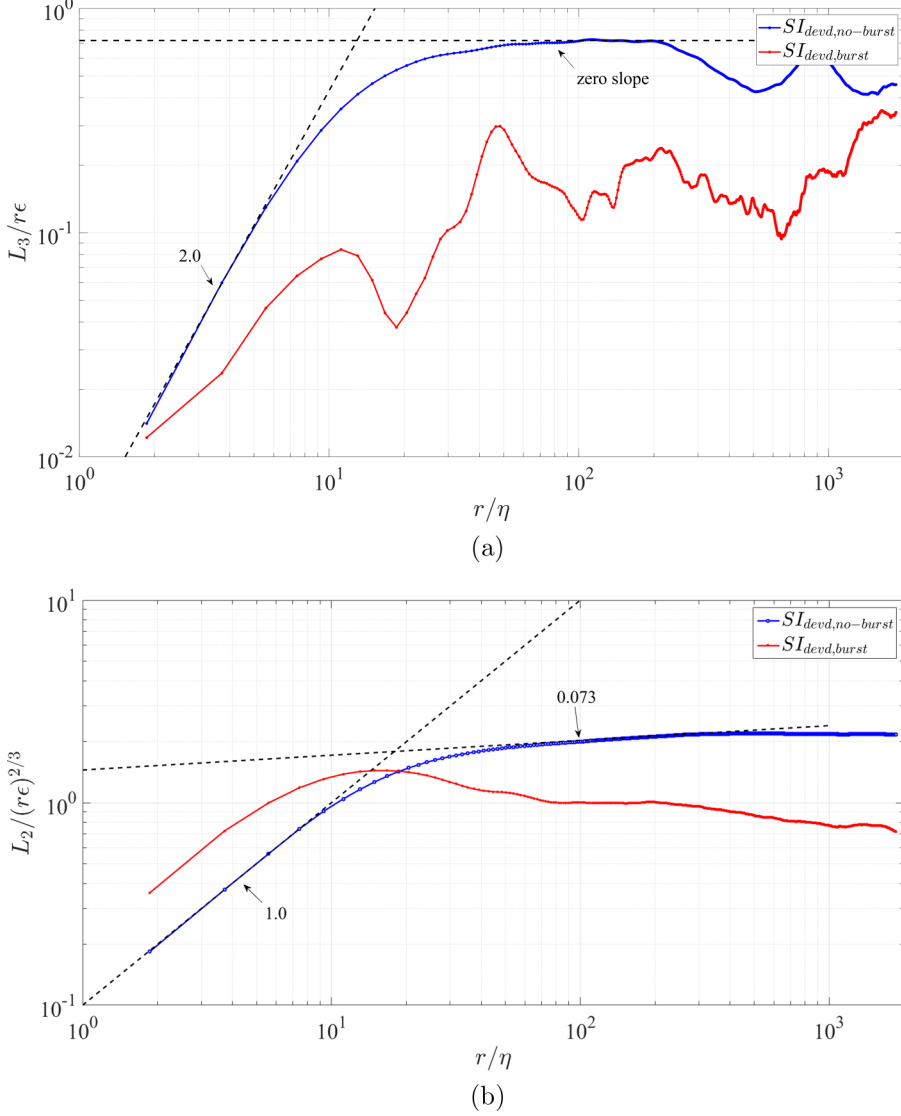
FIG. 5. Normalized according to KSSH third-order (a) and second-order (b) structure functions in field experiments computed using longitudinal velocity increment $\Delta u(x, r)$.

third- and second-order structure functions obtained in the field campaign are presented. As expected from the Kolmogorov equation, for the no-burst case, the normalized third-order longitudinal structure function approximately satisfied 4/5 law [Fig. 5(a)], with an approximately zero slope in the inertial subrange. In the viscous subrange, the slope of the normalized third longitudinal structure function is 2, or $L_3 \propto r^3$, indicating that $\Delta u(x, r) \propto r$. Figure 5(b) shows, however, for the same viscous subrange, $L_2/(r\varepsilon)^{2/3} \propto r$ or $L_2 \propto r^{5/3}$, indicating that $\Delta u(x, r) \propto r^{5/6}$ and not the expected $\Delta u(x, r) \propto r$.

While the above discussion concerned the no-burst case, it is noteworthy that in the viscous subrange similar slopes were obtained for the second-order structure function for the case with bursts [Fig. 5(b)]. No clear scaling was observed in the inertial subrange for datasets with bursts.

For the third-order structure functions, no clear scaling was observed either in the viscous or inertial subranges for the burst cases.

The near-zero negative (–0.13) slope of the canonical third-order structure in DNS [Fig. 3(a)] attests to similar dependence of second and third structure functions on r/η in the viscous subrange. Such behavior is expected, and has been observed in laboratory experiments with homogeneous flows (developed turbulence in a jet and past a cylinder) [13]; however, in the field data (Fig. 5) the dependences of second and third structure functions on r/η differ in the viscous subrange. This results in a slope of ≈ 0.5 in the viscous subrange for the third-order canonical structure function [Fig. 3(a)].

In the inertial subrange, the slope of the normalized second-order structure function is ≈ 0.073 [Fig. 5(b)], yielding a scaling exponent of 0.74, i.e., $L_2(r) \propto r^{0.74}$, instead of 0.667 expected from KSSH, $L_p(r) \propto (r\varepsilon)^{p/3}$. This explains the slope -0.1 in Fig. 3(a) of the third canonical structure function. From Eq. (2), it follows that $H_3(r) = L_3(r)/[L_2(r)]^{3/2} \propto r^{-0.11}$ (i.e., the exponent yielding $1-0.74 \times 1.5 = -0.11$, which is very close to -0.1). Similar results are found in the literature [11,12].

The above observations prompted investigations into all other (viable) even and odd structure functions for $\Delta u(x,r)$ and $|\Delta u(x,r)|$. Note that even moments are identical for both types of velocity increments. In the following, additional results are presented for the third- and first-order structure functions for modulus $|\Delta u(x,r)|$ (Fig. 6) and fourth- and sixth-order (Fig. 7) structure functions. The first-order structure function for $\Delta u(x,r)$ is identically zero. The third-order structure function for $\Delta u(x,r)$ was presented in Fig. 4(a).

It follows from Fig. 6 that the shapes in the viscous subrange ($r/\eta < 10$) are $L_1^* \propto r^{5/6}$ for the first-order and $L_3^* \propto r^{15/6}$ for the third-order structure functions, suggesting $|\Delta u(x,r)| \sim r^{5/6}$ as observed with second-order structure functions [Fig. 5(b)] and not to the separation r as observed with the third-order structure function for $\Delta u(x,r)$. In the inertial subrange, structure functions for both $|\Delta u(x,r)|$ and $\Delta u(x,r)$ almost follow Kolmogorov scaling, although a slight deviation was evident. As established earlier, in the viscous subrange, both third- and first-order structure functions evaluated for $|\Delta u(x,r)|$ with all datasets, including those with bursting events, have the same scaling [Figs. 6(a) and 6(b)]. In the inertial subrange, when bursting is present, the structure function is randomly varying and no definite scaling is observed.

The fourth- and sixth-order canonical structure functions in Fig. 7 confirm the same trend as observed above for first, second, and third structure functions for $|\Delta u(x,r)|$. In the viscous subrange, the velocity increment $|\Delta u(x,r)|$ is found to be proportional to $r^{5/6}$ for both datasets with and without bursts. This power law is also clearly confirmed for the fourth order and is nearly valid for the sixth-order structure function. In the inertial subrange, the fourth-order structure function approximately adheres to Kolmogorov scaling, and an anomaly becomes noticeable only when the sixth-order structure function is considered.

In particular, the slope of the fourth-order structure function in the inertial subrange is very small [Fig. 7(a)], about 3%, but unexpectedly positive, marginally exceeding KSSH prediction. The slope of the sixth-order structure function [Fig. 7(b)] in the same inertial subrange is negative, thus confirming the well-known anomaly [13–17] that the scaling exponent is lower than $p/3$ for high-order structure functions, which for our field experiments is $p \geqslant 5$. The deviation from the Kolmogorov scaling exponent noted in the literature [13–17] either obtained in the laboratory or DNS, however, is notably greater than that evaluated from our field data.

The normalized fifth-order structure functions based on the KSSH for $\Delta u(x,r)$ and $|\Delta u(x,r)|$ were calculated and are presented in Figs. 8(a) and 8(b). In the inertial subrange (around $r/\eta = 100$) the normalized fifth-order structure function [Fig. 8(a)] is undulating about the KSSH-predicted zero slope, however in the viscous subrange the structure function fluctuates randomly without a clear trend. No linear dependence between velocity increment $\Delta u(x,r)$ and separation r exists for the fifth-order structure function in contrast to that observed for the third-order structure function [Fig. 5(a)].
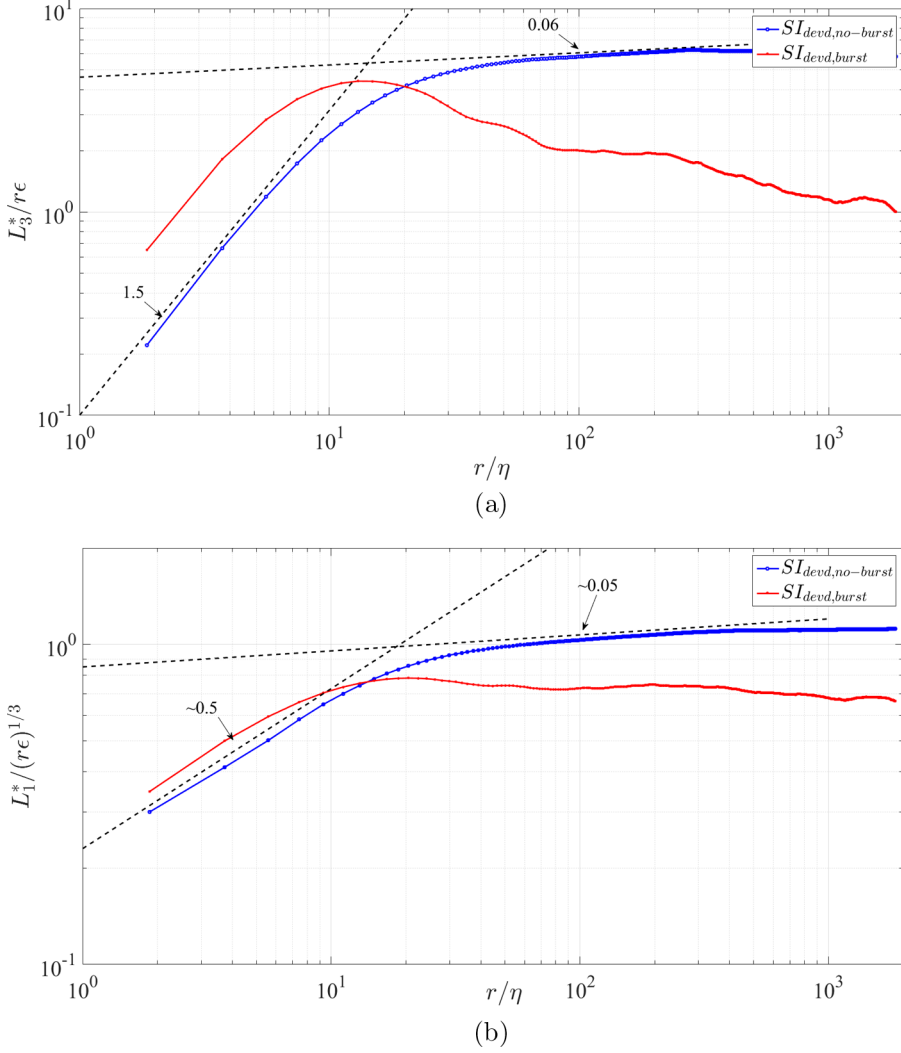
FIG. 6. Normalized odd third-order (a) and first-order (b) structure functions in field experiments computed using the modulus of the velocity increment.

The fifth-order normalized structure function for $|\Delta u(x, r)|$ behaves essentially different [Fig. 8(b)] from its $\Delta u(x, r)$ counterpart, with very smooth curves both in the inertial (around $r/\eta = 100$) and viscous subranges. The slope in the inertial subrange is approximately zero for the no-burst case, but a slight negative slope ($\approx -3\%$) is evident. The shape of this structure function in the viscous subrange ($r/\eta < 10$) is about $L_5^* \propto r^{25/6}$, corresponding to $|\Delta u(x, r)| \propto r^{5/6}$, the same as that observed for odd first- and third-order structure functions [Figs. 6(a) and 6(b)] and for all even structure functions studied here (second, fourth, and sixth). The same slope of 25/6 was observed in the viscous subrange for both burst and no-burst cases. In the inertial subrange, no clear scaling was observed with bursts.

The scaling exponents in the inertial and viscous subrange structure functions of different orders varying from first to sixth are summarized in Fig. 9. Although our field results in the inertial subrange do not contradict with those previously reported for HIT [11,19–23], there are modest qualitative discrepancies. The significant differences are in the small values of separation r/η in the
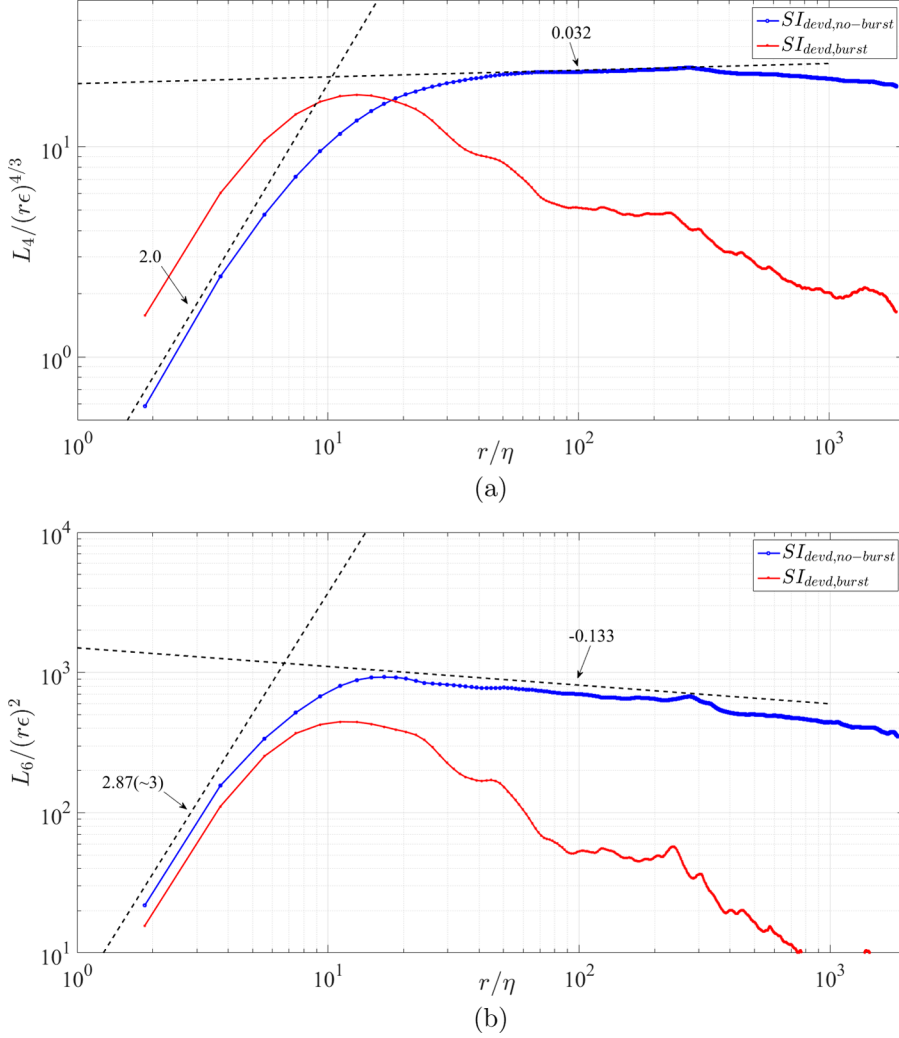
FIG. 7. Normalized according to KSSH even fourth-order (a) and sixth-order (b) structure functions in field experiments computed using the longitudinal velocity increment.

viscous subrange. A widely used assumption is that in the viscous subrange (which has received less attention in the past) both $\Delta u(x, r)$ and $|\Delta u(x, r)|$ vary similarly and nearly linearly with r [13,14]. This assumption is of practical interest for ESS, which suggests replacing εr of Kolmogorov normalization with the third-order structure function for $|\Delta u(x, r)|$.

According to our field results, the third-order structure functions in the viscous subrange behave as $\Delta u(x, r) \propto r$ and $|\Delta u(x, r)| \propto r^{5/6}$, revealing appreciably different behavior between the two. Only the last relation, $|\Delta u(x, r)| \propto r^{5/6}$, is confirmed for the fifth-order modulus structure function [Fig. 8(b)]; instead of linear dependence with r, the fifth-order conventional structure function for $\Delta u(x, r)$ [Fig. 8(a)] fluctuates randomly in the viscous subrange.

A surprising result is that in the viscous subrange *all* structure functions of the *modulus* of the velocity increment in our paper are described by the unique equation $\langle |\Delta u(x, r)|^p \rangle \propto r^{5p/6}$ for $p \in (1–6)$ (Fig. 9). The odd structure functions ($p = 1, 3,$ and 5) are definitely different for $\Delta u(x, r)$ than for $|\Delta u(x, r)|$. In particular, the first-order structure function for $\Delta u(x, r)$ is identically zero.
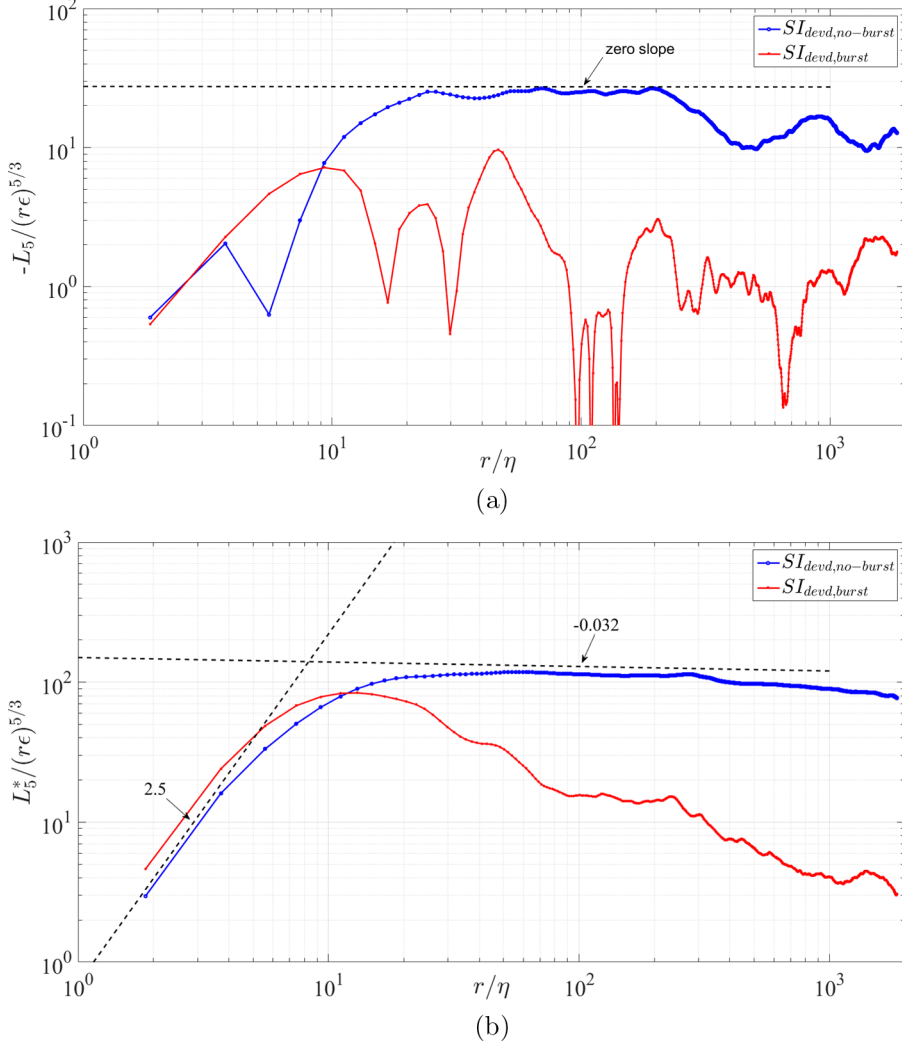
FIG. 8. Normalized fifth-order structure functions in field experiments computed using longitudinal velocity increment $\Delta u(x, r)$ (a) and its modulus (b).

The fifth-order structure function [Fig. 8(a)] in the viscous subrange did not allow determining the scaling exponent unambiguously. One could expect it to behave similarly to the third-order structure function (i.e., vary linearly with r). However, in our field experiments, disparities exist between third- and fifth-order structure functions, and it is highly probable that they are due to stable-stratification effects of the nocturnal ABL, as discussed below.

In our DNS of HIT, all scaling exponents of odd structure functions ($p = 3, 5,$ and 7) are approximately the same (Fig. 2) for $\Delta u(x, r)$ and $|\Delta u(x, r)|$. Additionally, in contrast to field results [Fig. 4(a)], the shape of the fifth-order structure function for $\Delta u(x, r)$ is smooth. Interestingly, in the viscous subrange calculations with field data, similar scaling exponents are also obtained for all structure functions for $|\Delta u(x, r)|$, including for data containing bursts. Conversely, for datasets with bursts, no definite scaling exponents are obtained in the inertial subrange with any type of velocity increment, including $|\Delta u(x, r)|$. This indicates that bursts mostly affect scales larger than those of the viscous subrange.
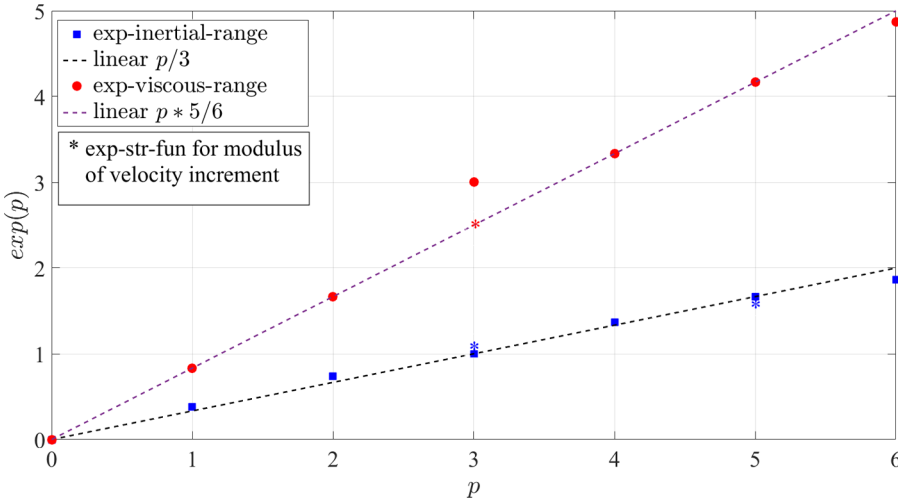
FIG. 9. Scaling exponents of the structure functions in the inertial and viscous subranges for the velocity increment and its modulus evaluated for field data. Stars indicate that different scaling exponents of structure functions (exp-str-fun) were obtained with odd third and fifth structure functions for velocity increments and their modulus.

The results for scaling exponents obtained in the present case of the stratified ABL (dubbed **str**) are presented in Table I along with their HIT counterparts (dubbed *hom*), with strong shear near the boundary (*sh*), theoretical predictions in accordance to the KSSH (*kssh*) in the inertial subrange, and linear dependence on r (*lin*) in the viscous subrange. As mentioned, it is commonly accepted that scaling exponents for the velocity increment and its modulus are practically the same across all subranges, and this claim has been partially verified in studies dealing with ESS of HIT [11,13]. Our results cast doubts on the *general* validity of this statement and, therefore, detailed results were presented for structure functions based on $\Delta u(x, r)$ and $|\Delta u(x, r)|$ for inertial and viscous subranges.

Naturally, only odd structure functions are relevant, since even functions are identical for $\Delta u(x, r)$ and $|\Delta u(x, r)|$ cases. The small differences between scaling exponents of third- and

TABLE I. Scaling exponents of the (structure) functions in the inertial and viscous sub-ranges for velocity increment and its modulus for datasets without bursts. *kssh* and *lin* are theoretical exponents $p/3$ in inertial and p in viscous subranges [18], *hom* and *sh* are experimental and DNS values in HIT and shear flows [28], **str** is for current field data measured under stratified conditions in nocturnal ABL. In viscous subrange, exponents for modulus of velocity increment yield $5p/6$ (NA: Not available from experiments or DNS).

Structure functions of order p	$\Delta u(x, r)$ Scaling exponents inertial subrange *kssh, hom,* **str***, sh*	$\|\Delta u(x, r)\|$ Scaling exponents Inertial subrange *kssh, hom, str, sh*	$\Delta u(x, r)$ Scaling exponents viscous subrange *lin, hom,* **str***, sh*	$\|\Delta u(x, r)\|$ Scaling exponents Viscous subrange *lin, hom, str, sh*
1	Function identically 0	0.333, 0.36, **0.38**, 0.44	Function identically 0	1.0, NA, **0.833**, NA
2	0.667, 0.70, **0.74**, 0.77		2.0, NA, **1.667**, NA	
3	1.0, 1.0, **1.0**, 1.0	1.0, NA, **1.06**, NA	3.0, NA, **3.0**, NA	3.0, NA, **2.50**, NA
4	1.333, 1.28, **1.334**, 1.17		4.0, NA, **3.333**, NA	
5	1.667, NA, **1.667**, NA	1.667, 1.54, **1.635**, 1.31	5.0, NA, **fluct**, NA	5.0, NA, **4.1667**, NA
6	2.0, 1.78, **1.867,** 1.44		6.0, NA, **4.87** NA	

fifth-order structure functions in the inertial subrange are within the uncertainty of the analysis, but in the viscous subrange the differences are substantial (Table I). In the inertial subrange, scaling exponents of the fourth-, fifth-, and sixth-order structure functions are considerably closer to Kolmogorov scaling (than their counterparts in flows with strong shear). The scaling exponent of the second-order structure functions, however, shows greater deviation from Kolmogorov scaling, thus contradicting the assumption of possible decrease of intermittency due to stable stratification.

The assumption of increased intermittency in *strong shear flow* seems plausible since the scaling exponents of all orders (first, second, fourth, fifth, and sixth) in the inertial subrange show an increased deviation from the KSSH-based scaling exponent obtained in HIT simulations and experiments. The exponent of the third-order structure function is 1 in *all* cases, in agreement with the Kolmogorov equation. In the viscous subrange, direct results for scaling exponents are not reported in published papers, but indirect results, including our DNS, where canonical and modified moments were calculated, show that the exponents for $\Delta u(x, r)$ and $|\Delta u(x, r)|$ for HIT are nearly the same.

The situation is different for stratified nocturnal ABL turbulence. The third structure function for the velocity increment in the viscous subrange shows predicted linear dependence, but the fifth-order structure function shows strong fluctuations thus precluding the determination of a scaling exponent. *All* structure functions for the modulus of the velocity increment, except the sixth order where a slight deviation was present, are yielding the scaling exponent $5p/6$.

The above results call for a plausible physical explanation. Note that the flow arriving at the ES-2 tower (equipped with the combo probe [52]) originated at the Granite Mountain slope [51,52] as a nocturnal katabatic flow. As it drains under stably stratified conditions, turbulence generated within is also advected and evolved, possibly becoming nearly HIT at ES2 [52,56], much the same way as in wind-tunnel stratified flows [46]. When stratification is very weak, the turbulence remains HIT type, but when stratification becomes stronger turbulence is buoyancy dominated, causing the PDF to be almost symmetrical. Our initial attempts to qualitatively assess the effect of moderate stratification on structure functions based on previous laboratory results by blending fluctuations from isotropic and anisotropic sectors at fine scales appear to explain the linear dependence between velocity increment and separation for the third-order normalized structure function (according to the KSSH) in the viscous subrange and why such dependence does not hold for the fifth-order normalized structure function. Such decomposition also allows obtaining different behavior for structure functions constructed for the absolute velocity increment $|\Delta u(x, r)|$. Presentation of this assessment is left for a future publication.

When laboratory grid generated HIT [46] is subjected to thermally generated stable stratification, turbulence becomes *anisotropic*, and the relevant controlling parameter of overall flow is the inverse of internal or turbulent Froude numbers, $\text{Fr} = \varepsilon/Nu'^2$ where u' is the rms of the velocity component, N is the buoyancy frequency, and ε is the rate of dissipation. The typical inverse Froude numbers assessed in our field experiments were $2-5$ [56], coincidentally in the same range as that observed in laboratory flows of [46], thus providing peripheral support for the notion of anisotropic turbulence at ES-2. Also note that the controlled laboratory results of [46] were obtained at relatively low $\text{Re}_\lambda \sim 20$–40 and that Fr does not specifically address the nuances of stratification effects, such as their penetration to viscous scales. As such, the observed in the field peculiar behavior of third canonical and modified structure functions and their departure from the HIT data results following from DNS need further investigation.

A rigorous attempt to separate isotropic and anisotropic contributions can be made in the framework of $SO(3)$ formalism by conducting the decomposition of appropriately measured structure or correlation functions into spherical harmonics [44,45,57]. However, this requires simultaneous multipoint measurement of high-frequency oscillating velocities and velocity derivatives and is left for future work.

IV. SUMMARY

The nocturnal stable boundary layer data acquired during the MATERHORN field program [51] were separated into no-bursts and bursts periods as in [52]. The no-burst field dataset as well as DNS datasets of HIT were used to study the structure functions of various order of the velocity increment $\Delta u(x, r)$ and its modulus $|\Delta u(x, r)|$.

The canonical structure function is obtained by normalizing higher-order structure functions of order p by the second-order structure function in power $p/2$ [Eq. (2)]. When structure functions of different orders are involved, this normalization can result in significant variation of the scaling exponent, for example, due to different anomalies caused by intermittency. Such effects are expected to magnify if the contributions from anisotropic sectors are accounted for [38,41], as in the case of shear and/or stratification. The computation of odd higher-order structure functions (third, fifth, and seventh) for $\Delta u(x, r)$ using four DNS datasets of HIT showed that although scaling exponents do not depend substantially on Re_λ the data are not collapsing in the inertial and viscous subranges, indicating that scaling used is unsatisfactory.

A modified normalization proposed for skewness of longitudinal velocity derivative $\partial u/\partial x$ by [53] involves the replacement of the second moment in the denominator of the canonical scaling with the same order third moment of the modulus $|\partial u/\partial x|$. This modified scaling was adopted for odd higher-order structure functions (third, fifth, and seventh) of $\Delta u(x, r)$, which were computed using DNS datasets of HIT. The results were striking: for all moments, a conspicuous collapse was achieved in the viscous and inertial subranges at all Re_λ used in the study, suggesting the efficacy of modified scaling for all moments. The collapse does not occur at larger scales, which is due to computational box boundaries and turbulence forcing at larger scales.

Detailed comparison of odd third- and fifth-order canonical and modified moments evaluated using field data without bursts with their DNS counterparts indicated a very good agreement in the inertial subrange $50 \leqslant r/\eta \leqslant 200$; for example, at $r/\eta = 100$, both field and DNS simulations at the highest Re_λ yield the same scaling exponents. In the viscous subrange, the third canonical and modified structure functions at small separations vary with separation as $\approx (r/\eta)^{0.5}$ in contrast to the approximately constant value exhibited by DNS.

The structure functions (of order p) in the nocturnal ABL are normalized according to the KSSH as $L_p(r)/(\varepsilon r)^{p/3}$, and for the third moment it yielded the predicted linear dependence $\langle \Delta u(x, r)^3 \rangle \propto r^3$ for smaller separations in the viscous subrange. In contrast, the second moment in the viscous subrange does not support the predicted r^2 dependence, but yielded $\langle \Delta u(x, r)^2 \rangle \propto r^{5/3}$. This explains the surprising scaling exponent of ≈ 0.5 for the canonical third-order structure function in the viscous subrange.

Since even moments are identical for the velocity increment and its modulus, in the viscous subrange the r dependence for the second moment could be extended for a general p-order moment as $\langle |\Delta u(x, r)|^p \rangle \propto r^{5p/6}$, which was (at least approximately) supported by our field data for all $p(1-6)$ used.

As implied from Fig. 5(a) and Fig. 6(a) above, in the viscous subrange of the stratified turbulence measured in the field the third-order structure functions of the velocity increment $\Delta u(x, r)$ and its modulus $|\Delta u(x, r)|$, normalized according to the KSSH, behave differently. The same data processing approximately confirmed 4/5 Kolmogorov law for the inertial subrange. The canonical and modified third-order structure functions computed for the same data showed very good agreement with their counterparts obtained in DNS for the inertial subrange; however, a substantial disparity was observed in the viscous subrange.

In the viscous subrange of DNS, the scaling exponent of the modified third-order structure function is close to zero, indicating that, in contrast to field observations, the scaling exponents for velocity increment $\Delta u(x, r)$ and for its modulus $|\Delta u(x, r)|$ for HIT are nearly the same.

As in the case of third order, the canonical and modified fifth-order structure functions computed using field data showed very good agreement with their DNS counterparts for the inertial subrange.

In the viscous subrange, both the canonical and modified fifth-order structure functions for field data were oscillating, and the scaling exponents could not be determined.

The field data set represents stratification-affected high Reynolds number turbulence in a katabatic flow in the nocturnal ABL [56]. An attempt was made to isolate stratification effects from the total turbulence field using a simple-minded assumption that the measured turbulence at 6 m above the ground is contributed by two uncorrelated effects: roughly HIT generated within the katabatic flow arriving from a nearby Granite mountain and motions due to stable temperature stratification at the measurement location (i.e., ES-2 tower). In the ABL, shear effects are substantial near the ground; however, at larger distances (e.g., 6-m height) turbulence tends toward HIT which can be affected by anisotropic tendency of stratification [46,47] that may even penetrate to fine scales. A simplified model based on blending of fluctuation contributions from isotropic and anisotropic sectors at fine scales appear to explain the linear dependence between velocity increment and separation for the third-order normalized structure function in the viscous subrange and why such dependence does not hold for the fifth-order normalized structure function (which is deferred to a future paper). In addition, such decomposition allows obtaining of different behavior for structure functions constructed for the absolute velocity increment $|\Delta u(x, r)|$. Considering all, we suggest that the more sophisticated SO(3) formalism [57] developed for decomposition of structure and/or correlation functions to separate contributions of isotropic and anisotropic sectors be attempted in future studies of anisotropy at small scales introduced by large scale effects such as stratification. Studies on small and viscous scales have become one of our foci because of the interest in understanding fog formation mechanisms, where spawning of water droplets occurs at Kolmogorov and sub-Kolmogorov scales of the ABL. We hope that this paper provides an entrée for future such work.

ACKNOWLEDGMENTS

[1] A. N. Kolmogorov, The local structure of turbulence in incompressible viscous fluid for very large Reynolds numbers, Dokl. Akad. Nauk SSSR **30**, 301 (1941).

[2] G. K. Batchelor and A. A. Townsend, The nature of turbulent motion at large wave-numbers, Proc. R. Soc. A **199**, 238 (1949).

[3] A. Y. S. Kuo and S. Corrsin, Experiments on internal intermittency and fine-structure distribution functions in fully turbulent fluid, J. Fluid Mech. **50**, 285 (1971).

[4] H. A. Rose and P. L. Sulem, Fully developed turbulence and statistical mechanics, J. Physique **39**, 441 (1978).

[5] U. Frisch, *Turbulence: The Legacy of A. N. Kolmogorov* (Cambridge University, Cambridge, England, 1995).

[6] A. Pouquet, Intermittent turbulence in a global ocean model, Physics **11**, 21 (2018).

[7] C. Rorai, P. D. Mininni, and A. Pouquet, Turbulence comes in bursts in stably stratified flows, Phys. Rev. E **89**, 043002 (2014).

[8] F. Feraco, R. Marino, A. Pumir, L. Primavera, P. D. Mininni, A. Pouquet, and D. Rosenberg, Vertical drafts and mixing in stratified turbulence: Sharp transition with Froude number, EPL **123**, 44002 (2018).

[9] T. Ishihara, T. Gotoh, and Y. Kaneda, Study of high-Reynolds number isotropic turbulence by direct numerical simulation, Annu. Rev. Fluid Mech. **41**, 165 (2009).

[10] T. Ishihara, K. Morishita, M. Yokokawa, A. Uno, and Y. Kaneda, Energy spectrum in high-resolution direct numerical simulations of turbulence, Phys. Rev. Fluids **1**, 082403(R) (2016).

[11] T. Gotoh, D. Fukayama, and T. Nakano, Velocity field statistics in homogeneous steady turbulence obtained using a high-resolution direct numerical simulation, Phys. Fluids **14**, 1065 (2002).

[12] R. Benzi, S. Ciliberto, R. Tripiccione, C. Baudet, F. Massaioli, and S. Succi, Extended self-similarity in turbulent flows, Phys. Rev. E **48**, R29 (1993).

[13] R. Benzi, S. Ciliberto, C. Baudet, G. R. Chavarria, and R. Tripiccione, Extended self-similarity in the dissipation range of fully developed turbulence, EPL **24**, 275 (1993).

[14] M. Briscolini, P. Santangelo, S. Succi, and R. Benzi, Extended self-similarity in the numerical simulation of three-dimensional homogeneous flows, Phys. Rev. E **50**, R1745 (1994).

[15] R. Benzi, S. Ciliberto, C. Baudet, and G. Ruiz Chavarria, On the scaling of three dimensional homogeneous and isotropic turbulence, Physica D **80**, 385 (1995).

[16] R. Benzi, L. Biferale, S. Ciliberto, M. V. Struglia, and R. Tripicccione, Generalized scaling in fully developed turbulence, Physica D **96**, 162 (1996).

[17] F. Anselmet, Y. Gagne, E. J. Hopfinger, and R. A Antonia, High-order velocity structure functions in turbulent shear flows, J. Fluid Mech. **140**, 63 (1984).

[18] M. Nelkin, What do we know about self-similarity in fluid turbulence? J. Stat. Phys. **54**, 1 (1989).

[19] Z. S. She and E. Leveque, Universal Scaling Law in Fully Developed Turbulence, Phys. Rev. Lett. **72**, 336 (1994).

[20] A. Arneodo, C. Baudet, F. Belin, R. Benzi, B. Castaing, B. Chabaud, R. Chavarria, S. Ciliberto, R. Camussi, F. Chillia, B. Dubrulle, Y. Gagne, B. Hebral, J. Herweijer, M. Marchand, J. Maurer, J. F. Muzy, A. Naert, A. Noullez, J. Peinke, F. Roux, P. Tabeling, W. van de Water, and H. Willaime, Structure functions in turbulence, in various flow configurations, at Reynolds number between 30 and 5000, using extended self-similarity, EPL **34**, 411 (1996).

[21] N. Boratav and R. B. Pelz, Structures and structure functions in the inertial range of turbulence, Phys. Fluids **9**, 1400 (1997).

[22] S. Grossmann, D. Lohse, and A. Reeh, Application of extended self-similarity in turbulence, Phys. Rev. E **56**, 5473 5, (1997).

[23] F. Belin, J. Maurer, P. Tabeling, and H. Willaime, Velocity gradient distributions in fully developed turbulence, Phys. Fluids **9**, 3843 (1997).

[24] K. R. Sreenivasan and B. Dhruva, Is there scaling in high-Reynolds number turbulence? Prog. Theor. Phys. Suppl. **130**, 103 (1998).

[25] S. Garg and Z. Warhaft, On small scale structure of simple shear flow, Phys. Fluids **10**, 662 (1998).

[26] X. Shen and Z. Warhaft, The anisotropy of the small scale structure in high Reynolds number ($R_\lambda \sim 1000$) turbulent shear flow, Phys. Fluids **12**, 2976 (2000).

[27] X. Shen and Z. Warhaft, Longitudinal and transverse structure functions in sheared and unsheared wind-tunnel turbulence, Phys. Fluids **14**, 370 (2002).

[28] F. Toschi, G. Amati, S. Succi, R. Benzi, and R. Piva, Intermittency and Structure Functions in Channel Flow Turbulence, Phys. Rev. Lett. **82**, 5044 (1999).

[29] R. Benzi, G. Amati, C. M. Casciola, F. Toschi, and R. Piva, Intermittency and scaling laws for wall bounded turbulence, Phys. Fluids **11**, 1284 (1999).

[30] F. Toschi, F. Leveque, and G. Ruiz-Chavarria, Shear Effects in Nonhomogeneous Turbulence, Phys. Rev. Lett. **85**, 1436 (2000).

[31] P. Gualtieri, C. M. Casciola, R. Benzi, G. Amati, and R. Piva, Scaling laws and intermittency in homogeneous shear flow, Phys. Fluids **14**, 583 (2002).

[32] C. M. Casciola, R. Benzi, P. Gualtieri, B. Jacob, and R. Piva, Double scaling and intermittency in shear dominated flows, Phys. Rev. E **65**, 015301(R) (2001).

[33] B. Jacob, A. Olivieri, and C. Casciola, Experimental assessment of a new form of scaling law for near-wall turbulence, Phys. Fluids **14**, 481 (2002).

[34] C. M. Casciola, R. Benzi, P. Gualtieri, B. Jacob, and R. Piva, Scale-by-scale budget and similarity laws for shear turbulence, J. Fluid Mech. **476**, 105 (2003).

[35] B. Jacob, L. Biferale, G. Iuso, and C. M. Casciola, Anisotropic fluctuations in turbulent shear flows, Phys. Fluids **16**, 4135 (2004).

[36] C. M. Casciola, P. Gualtieri, B. Jacob, and R. Piva, Scaling Properties in the Production Range of Shear Dominated Flows, Phys. Rev. Lett. **95**, 024503 (2005).

[37] C. M. Casciola, P. Gualtieri, B. Jacob, and R. Piva, The residual anisotropy at small scales in high shear turbulence, Phys. Fluids **19**, 101704 (2007).

[38] L. Biferale and M. Vergassola, Isotropy vs anisotropy in small-scale turbulence, Phys. Fluids **13**, 2139 (2001).

[39] L. Biferale and F. Toschi, Anisotropic Homogeneous Turbulence: Hierarchy and Intermittency of Scaling Exponents in the Anisotropic Sectors, Phys. Rev. Lett. **86**, 4831 (2001).

[40] L. Biferale, G. Boffetta, A. Celani, A. Lanotte, F. Toschi, and M. Vergassola, The decay of homogeneous anisotropic turbulence, Phys. Fluids **15**, 2105 (2003).

[41] I. Arad, B. Dhruva, S. Kurien, V. S. L'vov, I. Procaccia, and K. R. Sreenivasan, Extraction of Anisotropic Contributions in Turbulent Flows, Phys. Rev. Lett. **81**, 5330 (1998).

[42] I. Arad, V. S. L'vov, and I. Procaccia, Correlation functions in isotropic and anisotropic turbulence: The role of the symmetry group, Phys. Rev. E **59**, 6753 (1999).

[43] V. I. Belinicher and V. S L'vov, A scale-invariant theory of fully developed hydrodynamic turbulence, Zh. Eksp. Teor. Fiz. **93**, 533 (1987) [Sov. Phys. JETP **66**, 303 (1988)].

[44] V. S. L'vov, I. Procaccia, and V. Tiberkevich, Scaling exponents in anisotropic hydrodynamic turbulence, Phys. Rev. E **67**, 026312 (2003).

[45] L. Biferale and I. Procaccia, Anisotropy in turbulent flows and in turbulent transport, Phys. Rep. **414**, 43 (2005).

[46] S. T. Thoroddsen and C. W. Van Atta, The influence of stable stratification on small-scale anisotropy and dissipation in turbulence, J. Geophys. Res. **97**, 3647 (1992).

[47] S. T. Thoroddsen and C. W. Van Atta, Experiments on density-gradient anisotropies and scalar dissipation of turbulence in a stably stratified fluid, J. Fluid Mech. **322**, 383 (1996).

[48] P. Piccirillo and C. W. Van Atta, The evolution of a uniformly sheared thermally stratified turbulent flow, J. Fluid Mech. **334**, 61 (1997).

[49] K. H. Keller and C. W. Van Atta, An experimental investigation of the vertical temperature structure of homogeneous stratified shear turbulence, J. Fluid Mech. **425**, 1 (2000).

[50] S. E. Holt, J. R. Koseff, and J. H. Ferziger, A numerical study of the evolution and structure of homogeneous stably stratified sheared turbulence, J. Fluid Mech. **237**, 499 (1992).

[51] H. J. S. Fernando, E. R. Pardyjak, S. Di Sabatino, F. K. Chow, S. F. J. De Wekker, S. W. Hoch, J. Hacker, J. C. Pace, T. Pratt, Z. Pu *et al.*, The MATERHORN: Unraveling the intricacies of mountain weather, Bull. Am. Meteorol. Soc. **96**, 1945 (2015).

[52] E. Kit, C. Hocut, D. Liberzon, and H. J. S. Fernando, Fine-scale turbulent bursts in stable atmospheric boundary layer in complex terrain, J. Fluid Mech. **833**, 745 (2017).

[53] S. Sukoriansky, E. Kit, E. Zemach, S. Midya, and H. J. S. Fernando, Inertial range skewness of the longitudinal velocity derivative in locally isotropic turbulence, Phys. Rev. Fluids **3**, 114605 (2018).

[54] G. K. Batchelor and A. A. Townsend, Decay of vorticity in isotropic turbulence, Proc. R. Soc. A **190**, 534 (1947).

[55] E. Kit, A. Cherkassy, T. Saint, and H. J. S Fernando, In-situ calibration of hot-film probes using a co-located sonic anemometer: Implementation of a neural network, J. Atmos. Ocean Tech. **27**, 23 (2010).

[56] P. Conry, E. Kit, and H. J. S Fernando, Measurements of mixing parameters in atmospheric stably stratified parallel shear flow, Environ. Fluid Mech. **20**, 1177 (2020).

[57] S. Kurien and K. R. Sreenivasan, Measures of anisotropy and the universal properties of turbulence, in *New Trends in Turbulence: Nouveaux Aspects*, edited by M. Lesieur, A. Yaglom, and F. David (Springer-Verlag, Berlin, 2001), pp. 53–111.